Nuclear Instruments and Methods in Physics Research B 300 (2013) 62–67

Contents lists available at SciVerse ScienceDirect

Nuclear Instruments and Methods in Physics Research B

journal homepage: www.elsevier.com/locate/nimb

Elastic electron scattering cross sections at high momentum transfer

M. Vos [a,*], R.P. McEachran [a], E. Weigold [a], R.A. Bonham [b]

[a] Atomic and Molecular Physics Laboratories, Research School of Physics and Engineering, Australian National University, Canberra, ACT 0200, Australia
[b] Department of Biological, Chemical and Physical Sciences, Illinois Institute of Technology, 3101 South Dearborn Street, Chicago, IL 60616, USA

ARTICLE INFO

Article history:
Received 29 November 2012
Received in revised form 6 January 2013
Available online 13 February 2013

Keywords:
Elastic electron scattering
First Born approximation
Partial wave theory
Recoil energy

ABSTRACT

The elastic scattering cross section of keV electrons over large angles (>90°) is discussed. A comparison is made of the Rutherford cross section, the cross section obtained in the first Born approximation and that obtained by a partial wave calculation. The last approach differs significantly from the first two. For compounds, the recoil energy makes it possible to distinguish experimentally from which atom the electron has scattered. We compare the elastic peak ratio of H and O in water at several keV and for Hf and O in HfO_2 at 20–40 keV with the calculated ratios. Reasonable (but not perfect) agreement is obtained between the experiment and theory for the partial wave calculations.

1. Introduction and theoretical background

The elastic differential scattering cross section (DCS) of electrons is a cornerstone for the description of the transport of electrons in matter. It describes the probability of an electron being deflected by an atom over a specific angle. For small scattering angles θ the electron (energy E_0, momentum $\boldsymbol{k}_0$ before the collision, momentum $\boldsymbol{k}_1$ after the collision) interacts with many atoms and one has to take into account the interference of the waves emanating from different atoms. For larger θ values the momentum transfer $q = 2k_0\sin\theta/2$ becomes so large that $qR \gg 1$, (with R the interatomic separation) and then electron diffraction becomes negligible: one effectively scatters from a single atom and this atom acquires the transferred momentum $\boldsymbol{q} = \boldsymbol{k}_1 - \boldsymbol{k}_0$.

For very large q values, the recoil energy transferred to the scattering atom ($E_r = q^2/2M$ with M the mass of the scattering atom) becomes significant and results in a measurable decrease in the energy of the scattered electron. For example, for scattering from a hydrogen atom at 2 keV and $\theta = 135^\circ, E_r = 3.75$ eV. Under these conditions, when scattering from a molecule or a compound, the elastic peak splits up into several components, each corresponding to an atom with mass M, and quantitative analysis of the target composition becomes possible, provided that the elastic scattering cross sections are known [1–3]. Surface analysis using this method is often referred to as ERBS, electron Rutherford backscattering, as it has many similarities to (ion) Rutherford backscattering. By using the same experiment we can, of course, test our understanding of the elastic DCS, when the composition of the sample is known.

Until recently elastic differential cross section measurements were restricted to noble gases and some metals with high vapor pressure, see Ref. [4] for an overview. These gas-phase measurements employ momentum transfers up to 15 a.u., but usually much less. ERBS is done at significantly higher momentum transfer, and can be done both in the gas phase and from surfaces.

It is thus of great interest to establish what is the appropriate elastic scattering cross section at large momentum transfer. As the technique is called electron Rutherford backscattering, a logical first cross section to consider is the Rutherford cross section. It works very well for MeV ion scattering, but how does it describe electron scattering at many keV's? The DCS for scattering from a nucleus with atomic number Z is given by (we work in atomic units throughout):

$$\frac{d\sigma}{d\Omega} = \frac{4\gamma^2 Z^2}{q^4} \tag{1}$$

with $\gamma = (1 - v^2/c^2)^{-1/2}$. This formula describes the scattering from a bare nucleus. It is a peculiarity of the Coulomb potential that the DCS of Eq. 1 is obtained both in the first Born approximation (FBA) and the exact solution [5], i.e. the contributions from the higher order Born terms cancel.

In reality the scattered electron sees a potential $V(r)$ that is due to the nucleus and the target electrons. This potential is, except very close to the nucleus, completely different from the Coulomb potential. (see Fig. 1 top left panel). In the FBA the DCS is given by (see e.g. [6]):

* Corresponding author. Tel.: +61 2 6125 4985.
E-mail address: Maarten.Vos@anu.edu.au (M. Vos).

0168-583X/$ - see front matter © 2013 Elsevier B.V. All rights reserved.
http://dx.doi.org/10.1016/j.nimb.2013.01.043

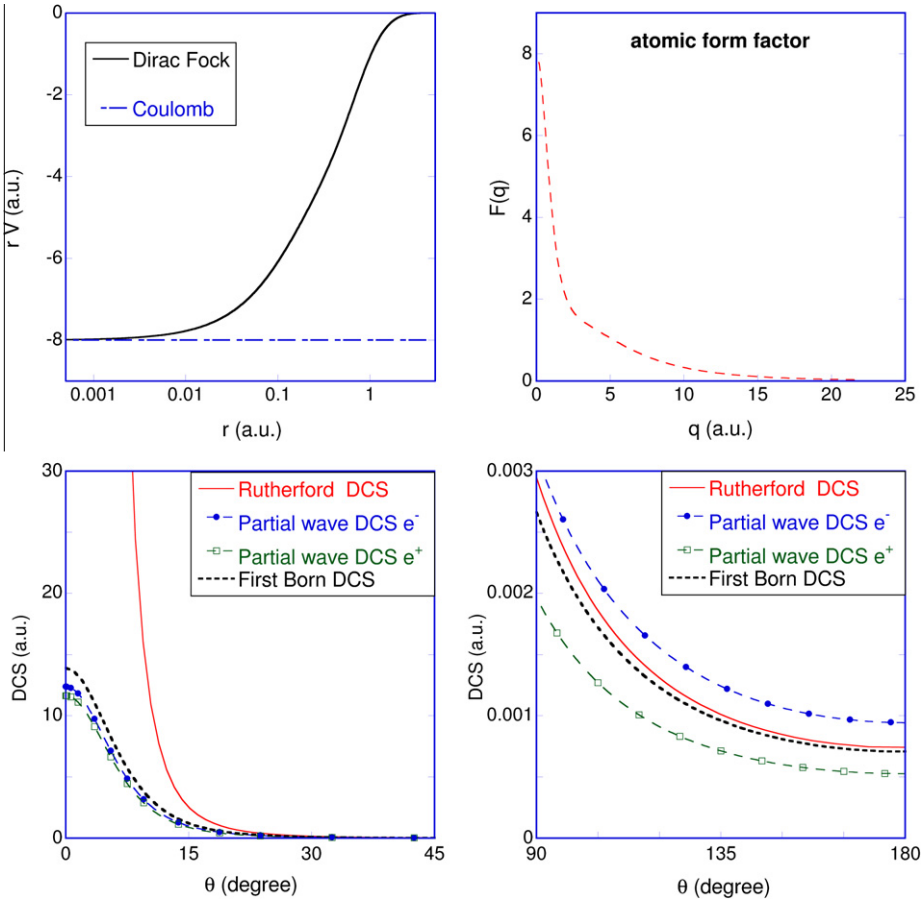

Fig. 1. In the top-left panel we compare r times the static potential V for a bare oxygen nucleus (Coulomb potential) and a neutral O atom using the numerical Dirac–Fock charge density [7]. The atomic form factor $F(q)$ is shown in the top right panel. In the FBA the DCS of an atom is given by replacing Z in the Rutherford formula by $Z - F(q)$. In the lower panels we compare, for 2 keV scattering from O, the Rutherford cross section with the FBA and the partial wave calculation. The latter gives different results for positrons and electrons. For large scattering angles the DCS in the partial wave formalism is, for electrons, substantially larger than the Rutherford or FBA cross section.

$$\frac{d\sigma}{d\Omega} = \frac{1}{4\pi^2}\frac{k_1}{k_0}\left(\int e^{iq\cdot r}V(r)dr\right)^2. \tag{2}$$

Here we consider scattering from the static potential, and neglect exchange scattering, the effect of polarization of the atom by the scattering particle, and absorption (the reduction of the elastically scattered flux due to inelastic excitation and ionization of the scattering atom). For keV electrons, scattering over large angles, the effects of exchange and polarisation are negligible but absorption influences the scattering cross section somewhat, as we will see later.

The electric field at a distance r from the nucleus is proportional to the total charge within the sphere of radius r. The Fourier transform of the electron charge distribution is a central ingredient in the theory of X-ray diffraction and is called the atomic form factor $F(q,Z)$. This makes it possible to rewrite Eq. 1 as

$$\frac{d\sigma}{d\Omega} = \frac{4\gamma^2(Z - F(q,Z))^2}{q^4}. \tag{3}$$

As an example let us consider 2 keV electrons scattering from an oxygen atom. The atomic form factor $F(q,Z)$ of element Z has been parameterized [8]. For O $F(q,Z)$ is plotted in Fig. 1 (top right panel). For scattering of e.g. 2 keV electrons over 135°, q = 22.4 a.u. The value of $F(q,Z)$ is then very small and reduces the Rutherford cross section by only 1%, and this seems to justify the use of the Rutherford formula.

However, it should be noted that the potential shape of the screened potential is completely different from the Coulomb potential of the bare nucleus. For the Coulomb potential the contributions of the higher order Born terms cancel. This may not be the case for the screened potential. Hence we also calculated the DCS using the partial wave formalism, which should give a complete description of the scattering process, provided a sufficient number of partial waves is used. For this we used the ELSEPA package [7], and calculated the DCS for both positrons and electrons (see Table 1). As a check a comparison was made with the partial wave

Table 1
The differential elastic scattering cross sections (in a.u.) for a scattering angle of 135°, as calculated using ELSEPA used in this paper.

E_0 (keV)	H		O		Hf	
	No abs.	Incl. abs.	No abs.	Incl. abs.	No abs.	Incl. abs.
1.5	2.87E-05	2.74E-05	2.28E-03	2.02E-03	–	–
2.0	1.61E-05	1.55E-05	1.24E-03	1.12E-03	–	–
2.5	1.02E-05	9.95E-06	7.76E-04	7.06E-04	–	–
3	7.09E-06	6.91E-06	5.28E-04	4.84E-04	–	–
20	–	–	1.03E-05	1.00E-05	1.79E-03	1.70E-03
30	–	–	4.48E-06	4.40E-06	7.88E-04	7.55E-04
40	–	–	2.48E-06	2.44E-06	4.38E-04	4.22E-04

calculations using the code of Chen et al. [9] and excellent agreement with ELSEPA was found under these conditions.

The various DCS are shown in the lower half of Fig. 1 for the case of 2 keV scattering from O. For small scattering angles the Coulomb potential diverges, but the partial wave and the FBA results resemble each other. At large scattering angle, the partial wave DCS for positrons and electrons differ, but the Rutherford and FBA results (obtained either by direct Fourier transform (Eq. 2) or using the X-ray form factor (Eq. 3)) are very similar.

Within the FBA the cross section is proportional to the square of the projectile-target interaction, and hence the DCS of positrons and electrons are the same. The very considerable difference in the partial wave calculation is thus a clear proof of the inadequacy of the FBA. By using semi-classical arguments one can make the different behavior of positrons and electrons plausible. The attractive potential for electrons tends to focus the electron flux towards the nucleus, making small impact parameter collisions with the corresponding large deflections angles more likely. For positrons it is the other way around.

If we do the same calculations for hydrogen at 2 keV then the difference between the partial wave solution for positron and electron scattering is less than 3% at backward angles, and the DCS is very close to the Rutherford cross section. Thus, for an electron scattering measurement from water at 2 keV and 135°, we would, according to the partial wave calculations, expect the ratio of the H and O elastic peak (separated due to different recoil energies) to be not $2Z_H^2 : Z_O^2 = 1 : 32$ as predicted by Rutherford formula but closer to 1:39. A (currently hypothetical) identical experiment, but using positrons, should give a value close to 1:23. Note that these numbers will change somewhat if we include absorption in the calculations.

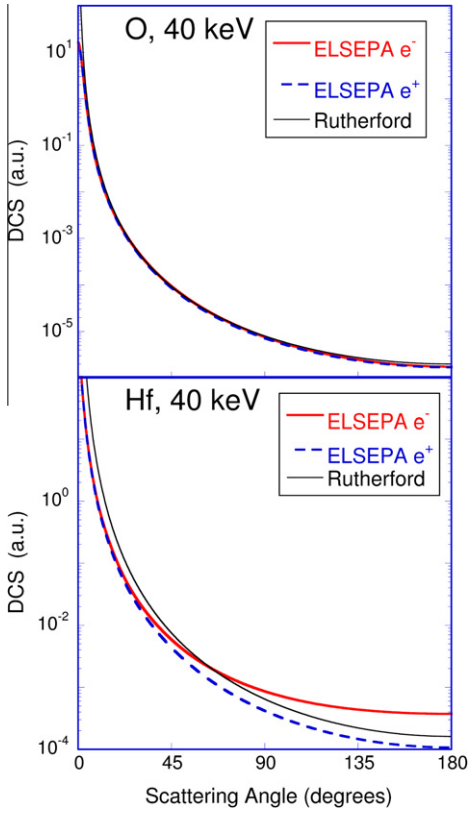

Fig. 2. The DCS of O and Hf at 40 keV, as calculated for both positrons and electrons using the partial wave formalism, and from the Rutherford formula.

If we increase the electron energy E_0 then the differences between all theories decrease. However, for heavier elements the differences persist up to much higher energies. In order to illustrate this we calculated the DCS of O and Hf at 40 keV (Fig. 2). Now the FBA, Rutherford and the partial wave formalism all give very similar answers for O (except near 0°), but for the much heavier Hf the deviations are still very strong, and there is a difference of about a factor of 3 between the DCS of positrons and electrons at 135° (see Table 1).

With the realization that the elastic peak of molecules and compounds splits up at high momentum transfer due to the different recoil energies for electrons scattering from different masses [1,2], there is a new interest in the elastic DCS of atoms at large momentum transfer. Can we interpret the data based on the Rutherford formula (i.e. cross section is proportional to Z^2), or do we have to use the partial wave formalism? From the compilation of measured elastic DCS in Ref. [4] there appears to be no DCS measurements under the conditions that recoil energies are important (i.e. $q \geqslant 15$ a.u.). In this paper we present measurements on water at energies between 1 and 3 keV and on HfO_2 between 20 and 40 keV. Under these experimental conditions the DCS for the light elements, as calculated with ELSEPA, are in good agreement with the Rutherford formula, but there is clear disagreement for the heavy elements. Is the theoretical result that the DCS of the heavy element exceeds the Rutherford cross section supported by the experiment? Note that naively most people would expect the disagreement between the measured cross section and the Rutherford cross section to be the other way around: i.e. expect that screening decreases the cross section of the heavier element as the scattering electron sees, due to screening, effectively a lower Z value, especially for the heavy element.

2. Experimental details

Two spectrometers were used. For both spectrometers the scattering angle was 135°. One spectrometer for the H_2O experiment used incoming energies between 1 and 6 keV. This experiment was described extensively in a separate paper, mainly focusing on peak shape and isotope effects [10]. The other spectrometer operated at E_0 between 20 and 40 keV and was used for the HfO_2 experiment. This spectrometer was also described in detail elsewhere [3]. HfO_2 is extremely well studied material as it plays a central role in the ongoing effort to reduce the dimensions of electronic devices [11]. The 20 nm thick HfO_2 layers were grown by atomic layer deposition on a silicon substrate, using the methods developed for device fabrication, and are expected to be pure and very close to the nominal stoichiometry. No attempt was made to clean the surface. In both cases the main experimental difficulty is the determination of the elastic peak area of a small low-Z component next to a very intense high-Z component, even for the favorable cases chosen here, where the number of the low-Z atoms is twice that of the high-Z atoms. This is exasperated by the fact that the peak of the low-Z component is much broader than the peak of the high-Z component as the lighter component is more affected by Doppler broadening. The maximum height of the low-Z peak is in practice ≈200× less than the height of the high-Z peak. The determination of the area of the low-Z peak above the 'background' due to the tail of the high-Z peak requires great care.

The experimental energy resolution of both spectrometers is close to 0.3 eV full-width-half-maximum (this includes the energy spread of the incoming beam). Unless otherwise stated the peak due to the heaviest element (mass M) is aligned with its recoil energy ($q^2/2M$) as the exact zero of the energy scale is unknown. The electron beam current used varies from 200 nA for the water vapor

experiments to 7 nA for ice and HfO_2. The vapor measurements took several days, the thin film spectra required approximately 2 h.

3. Experimental result

3.1. H_2O

In the top panel of Fig. 3 we show an example of a water (vapor) spectrum taken at 2 keV. The spectrum consists of two peaks, a main peak at low energy loss, and a second peak, considerable broader at larger energy loss. The first peak is interpreted as being due to scattering from O, the second due to scattering from H. The observed O–H peak separation of 3.53 eV is indeed very close to the calculated difference in recoil energy for scattering from O and H atom (3.49 eV). The spectrum is fitted with Gaussians. In order to get an accurate description of the O peak one needs 3 Gaussians of different widths, centered at slightly different positions. The H peak can in practice be described by a single Gaussian. In Fig. 3, top panel we show the total fit, as well as the total fit with the H component removed. These measurements were done at several energies and for both vapor and ice. The ice spectra are very similar to the vapor spectra, except additional loss structures above 8 eV due to inelastic excitations in the ice layer. For more details see Ref. [10].

The resulting intensity ratios $I_O : I_H$ are displayed in the lower panel of Fig. 3 and compared to the intensity ratios calculated from the various cross sections. The ratio based on the Rutherford cross section is always below the experimentally observed one. The ELSEPA program was used to calculate the DCS in two different ways: by using only the static potential or by using the static potential *plus* an optical potential describing absorption due to inelastic processes (see also Table 1). Agreement with the former is better than the latter.

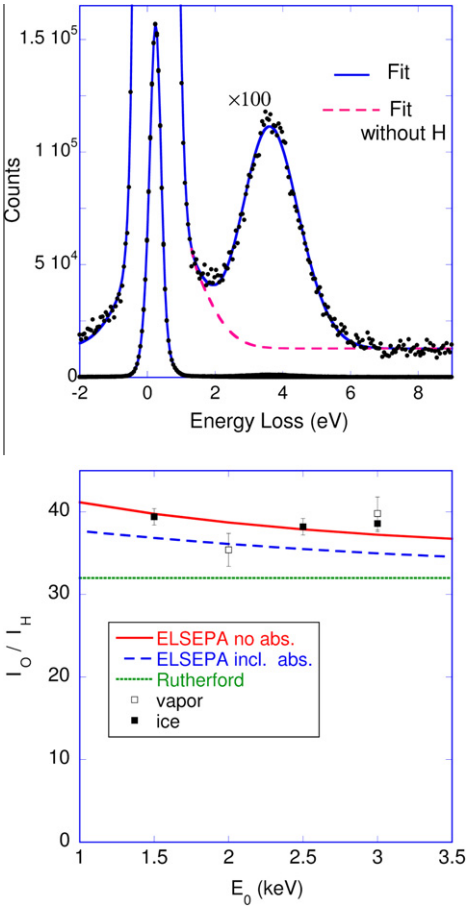

Fig. 3. The top panel shows an example of a 2 keV water (vapor) spectrum with an O and H elastic peak. The peak area ratio is plotted in the lower panel, together with the calculated ratio based on the partial wave formalism (with and without absorption) as well as the Rutherford cross section.

3.2. HfO_2

For HfO_2 we expect that the intensity of the low-Z signal relative to the high-Z signal to be even smaller than for H_2O. Therefore it is crucial to investigate the shape of the background. For this we did a 5 keV measurement as shown in Fig. 4. At this energy the separation of the Hf and O peak is only 0.5 eV and the two peaks are not resolved. The spectrum shows a single elastic peak, followed by a fairly constant background. At larger energy loss the background starts rising linearly. By fitting the spectrum with a constant and linear term, we find the onset of the rising background is at 5.7 eV. This onset is often taken as a measure of the bandgap, and our results here are in reasonable agreement with transmission EELS experiments of HfO_2 (between 5.3 and 5.8 eV, depending on the crystal structure [12]) and reflection EELS experiments of Jin et al. (5.5 eV [13]).

For the 5 keV measurement shown in Fig. 4 the experiment is fairly surface sensitive, but if we increase the incoming energy (in order to separate the elastic peak in components corresponding to different elements) we probe thicker layers. The estimate of the inelastic mean free path λ_i of 40 keV electrons in HfO_2, based on the Tanuma–Powell–Penn formula is 34 nm. (18.5 nm at 20 keV) [14]. Some of the incoming and outgoing electrons will now travel through the HfO_2 layer without inelastic excitations, and hence the Si elastic peak could also be visible.

At 40 keV the different elastic peaks are indeed resolved, as is seen in Fig. 5. This spectrum was fitted with three components, and the peak separation was consistent within the statistical accuracy with contributions of Hf, Si and O. This is an experimental verification that the large majority of the electron trajectory are close to 'V-shaped', i.e. their trajectory has only one large-angle deflection, very close to the angle between the incoming and outgoing beam. For these 'V-shaped' trajectories the inelastic mean free path is a good approximation of the attenuation length.

If the incoming beam is directed along the surface normal then the total path length l (incoming plus outgoing trajectory) through

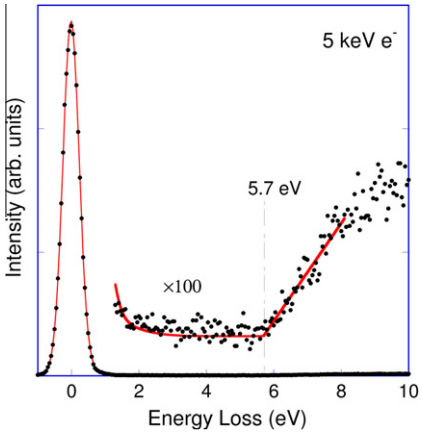

Fig. 4. The fitting of the spectrum of HfO_2 for E_0 = 5 keV. The Hf and O elastic peaks are not separated under these conditions and the elastic peak is aligned with zero energy loss. The background is first rather constant but increases for energy losses above 5.7 eV due to electrons which have scattered elastically from an atom and have created an electron–hole pair.

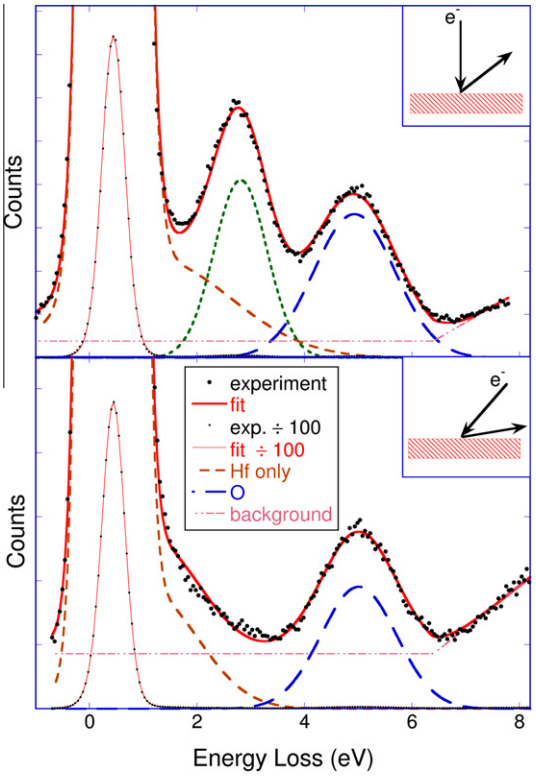

Fig. 5. Examples of spectra of 20 nm HfO_2 on Si taken at 40 keV. The top panel is for the incoming beam along the surface normal. Here the contribution of the Si substrate is still visible as a peak near 2.8 eV energy loss. The bottom panel shows the spectrum after rotating the sample by 35°. The outgoing trajectories are then rather glancing and the measurements are more surface sensitive. Now the Si peak is absent. The Hf, Si and O components and the background as obtained from the fitting procedure are shown as well. The inserts sketch the measurement geometry.

the 20 nm thick HfO_2 layer for electrons backscattered from Si is 48 nm (length incoming trajectory 20 nm, length outgoing trajectory $20/\sin(45^\circ) \approx 28$ nm). Thus the Si signal will be attenuated by a factor of $e^{-l/\lambda_i} = 0.24$. As the Si cross section is about 3 times larger than the O cross section, its contribution to the spectrum is expected to be of the same order as the O contribution. This is indeed the case, as seen in Fig. 5. As is clear from this figure, ERBS is a very good tool for probing the thickness of oxide layers. Standard XPS measurements would not reveal the substrate under a 20 nm thick HfO_2 layer and hence cannot be used to measure the thickness of such an oxide layer. The unique possibilities of ERBS as a quantitative analysis technique for surface layers of intermediate thicknesses is an important motivation for us to study these cross sections.

The amount of Si visible in the spectrum is not important for our discussion of the cross section ratio of Hf and O. A good fit of the spectrum is required only in order to extract the O peak area with good precision. The huge Hf peak area is not affected by how we deal with the small Si peak present.

In order to simplify the fitting procedure we also took a spectrum with the sample rotated by 35°, in such a way that the direction of the detected electrons was glancing (10° relative to the surface). The effective thickness of the HfO_2 layer is now 140 nm, reducing the Si substrate intensity to 1.5% of the uncovered Si intensity. Indeed now we can fit the spectrum with only a Hf and an O component, as can be seen in the lower panel of Fig. 5.

The Hf peak appears, at first sight, to be a reasonable approximation of a Gaussian, but if we enlarge the vertical scale by a factor of 100, then it is apparent that it is rather asymmetric and has a tail at the high-energy loss side. This tail is often seen and depends on

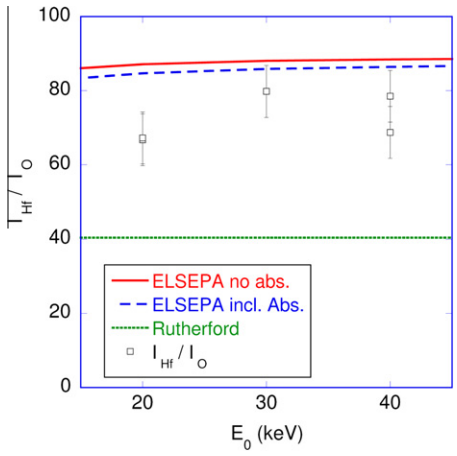

Fig. 6. A comparison of the Hf to O intensity ratio with the expectation based on the various calculated cross sections for the E_0 values as indicated.

the exact sample location and lens setting. This complicates the fitting procedure somewhat. Thus the main Hf peak has to be fitted by up to 3 Gaussian components to get a good description. The Si peak shape is well known [2], hence the only additional variables in the fitting procedure is the precise shape of the Hf tail and O peak width. For the rotated sample, spectra were also taken at an incoming energy E_0 of 20 and 30 keV.

The intrinsic width of the O peak, in terms of the standard deviation σ ($\sigma \approx \Gamma/2.355$, with Γ the full width at half maximum for a Gaussian peak), is given by: [15]

$$\sigma = \sqrt{\frac{4}{3}\overline{E_r}\,\overline{E_{kin}}}, \tag{4}$$

where $\overline{E_r}$ is the recoil for scattering from a stationary atom and $\overline{E_{kin}}$ the mean kinetic energy of the scattering atom. $\overline{E_r}$ increases linearly with E_0. We get a good fit of the spectra at 20, 30 and 40 keV, if we assume that $\overline{E_{kin}} = 72$ meV and fix the width to the value calculated according to Eq. 4. This value of $\overline{E_{kin}}$ is comparable to the mean kinetic energy of O in SiO_2 [2].

By using the background shape from the 5 keV measurement and fixing the widths of the Si (when required) and O peak, as described above, we have a fairly constrained fitting procedure. The peak area ratios $I_{Hf} : I_O$ obtained are shown in Fig. 6. Clearly the Rutherford cross section underestimates $I_{Hf} : I_O$, while the partial wave calculation is somewhat better, but it overestimates the ratio somewhat.

4. Conclusion and discussions

There has been some confusion about which DCS is required to describe the intensities in ERBS spectra. The Rutherford cross section is one option. Within the FBA screening reduces the DCS relative to the Rutherford cross section. However, partial wave calculations show that, *for electrons*, the DCS is larger than the Rutherford cross section. This should not be a complete surprise as the potential shape is completely different for an atom and a bare nucleus, and the FBA is known not to describe the cross sections well. This can be a substantial effect, e.g. in the case of HfO_2 there is a factor of 2 difference between the Rutherford and the partial wave cross section ratio.

Partial wave calculations were done with and without considering absorption. Absorption moves the intensity ratio somewhat closer to the expectation based on the Rutherford cross section, as it affects scattering from the heavy atom more than from the light atom, but a substantial difference remains. For H_2O the exper-

imentally observed intensity ratio scatters around the theory without absorption and the ratio is somewhat too high if we take absorption into account. We want to caution against the view that these measurements show that absorption does not play a role under these conditions.

For HfO_2 the experimentally observed intensity ratios are in between the values calculated by the Rutherford formula and the partial-wave theory. The intensity ratios based on the partial-wave calculations are closer to the experiment but tend to overestimate $I_{Hf} : I_O$ ratio somewhat. Here absorption (when using the same (default) value for the absorption strength parameter in ELSEPA of 2 for both O and Hf) modifies the ratio even less. The presence of surface adsorbates, always present without in situ cleaning (water, CO and hydrocarbons) could be the cause of part of the discrepancy as they will cause additional intensity near the O peak. For these incoming energies their contribution is expected to be less than the difference observed.

In not a single case did we see an intensity ratio less than that predicted by the Rutherford cross section. Thus the naive picture that screening of the nuclear charge by core electrons reduces the DCS of the heavy atom more than the DCS of light atoms is clearly wrong.

It would be of great interest to do these experiments with positrons, as the peak ratio should be completely different in that case. This is currently not a practical experiment as it requires a beam current of the order of 1 nA.

There are possible complications due to multiple scattering for the case of electron scattering from thin films. However, Monte Carlo simulations have, so far, not shown a dramatic effect of multiple scattering on the actual shape of the spectrum [15]. It could be different for these compounds consisting of light and heavy atoms such as HfO_2, and investigating this case using Monte Carlo techniques would certainly be worthwhile. However, the fact that the spectra can be fitted using the calculated Hf–O peak separation for scattering over 135° argues strongly that trajectories with multiple large-angle deflections are in the minority as the total recoil loss of trajectories with multiple large-angle deflection are not expected to peak at that specific energy loss.

Another fact we want to stress is that the ELSEPA code assumes free atoms, and the atoms studied here are part of a molecule or solid. We do not expect that this 'atomic' approximation is a source of significant errors for the current scattering conditions.

Finally, we want to make some remarks about the peak shape. Within the FBA there is a clear link between the peak shape as observed in electron scattering and in neutron scattering [16]. In both cases the peak shape is then proportional to the dynamical structure factor $S(q,\omega)$ with ω the energy loss. From the calculations we have done in the context of this paper we conclude that, for incoming energies E_0 where the recoil shift is substantial (1–2 eV or more), the FBA gives a good description of the cross section, and a comparison with neutron results appears valid.

At high momentum transfer the final state of the scattering atom (when the plane-wave-impulse approximation applies) $S(q,\omega)$ becomes simply a Doppler profile of the atomic motion. However, when we consider the present case of scattering from Hf at 40 keV the situation could be problematic. Here the energy transferred in the collision (0.4 eV) is probably too small for the plane-wave-impulse approximation to be valid, so the shape cannot be interpreted as a Doppler profile of the atomic motion. The DCS is also not described well by the FBA, so there is reason to doubt that in this case neutron and electron measurements would resemble each other, as the latter is not necessarily proportional to $S(q,\omega)$. In particular the corrections to the impulse approximation, as described by Sears [17], are expected to fail under these conditions.

Acknowledgements

The HfO_2 sample was kindly provided by R. Elliman and D. Venkatachalam (EME department, Australian National University). The authors want to thank R. Moreh for stimulating discussions. This research was made possible by funding of the Australian Research Council.

References

[1] M. Vos, Observing atom motion by electron-atom Compton scattering, Phys. Rev. A 65 (2001) 12703, http://dx.doi.org/10.1103/PhysRevA.65.012703.
[2] M. Went, M. Vos, Investigation of binary compounds using electron Rutherford back scattering, Appl. Phys. Lett. 90 (2007) 072104, http://dx.doi.org/10.1063/1.2535986.
[3] M. Went, M. Vos, Rutherford backscattering using electrons as projectiles: underlying principles and possible applications, Nucl. Instr. Meth. Phys. Res. B 266 (2008) 998–1011, http://dx.doi.org/10.1016/j.nimb.2008.01.059.
[4] F. Salvat, optical-model potential for electron and positron elastic scatteing by atoms, Phys. Rev. A 68 (2003) 012708, http://dx.doi.org/10.1103/PhysRevA.68.012708.
[5] E. Merzbacher, Quantum Mechanics, 2nd ed., John Wiley & Sons Ltd., 1970.
[6] L. van Hove, Correlations in space and time and Born approximation scattering in systems of interacting particles, Phys. Rev. 95 (1954) 249–262, http://dx.doi.org/10.1103/PhysRev.95.249.
[7] F. Salvat, A. Jablonski, C.J. Powell, ELSEPA Dirac partial-wave calculation of elastic scattering of electrons and positrons by atoms, positive ions and molecules, Comput. Phys. Commun. 165 (2005) 157–190, http://dx.doi.org/10.1016/j.cpc.2004.09.006.
[8] T.G. Strand, R.A. Bonham, Analytical expressions for the Hartree–Fock potential of neutral atoms and for the corresponding scattering factors for x rays and electrons, J. Chem. Phys. 40 (1964) 1686, http://dx.doi.org/10.1063/1.1725380.
[9] S. Chen, R.P. McEachran, A.D. Stauffer, Ab initio optical potentials for elastic electron and positron scattering from the heavy noble gases, J. Phys. B At. Mol. Opt. Phys. 41 (2008) 025201, http://dx.doi.org/10.1088/0953-4075/41/2/025201.
[10] M. Vos, E. Weigold, R. Moreh, in press. Elastic electron scattering from water vapor and ice at high momentum transfer. J. Chem. Phys. 138 (2013) 044307, http://dx.doi.org/10.1063/1.4775810.
[11] J. Choi, Y. Mao, J. Chang, Development of hafnium based high-k materials: a review, Mater. Sci. Eng. R Rep. 72 (6) (2011) 97–136, http://dx.doi.org/10.1016/j.mser.2010.12.001.
[12] M.C. Cheynet, S. Pokrant, F.D. Tichelaar, J.-L. Rouviere, Crystal structure and band gap determination of HfO_2 thin films, J. Appl. Phys. 101 (2007) 054101, http://dx.doi.org/10.1063/1.2697551.
[13] H. Jin, S.K. Oh, H.J. Kang, S. Tougaard, Electronic properties of ultrathin HfO_2, Al_2O_3, and Hf–Al–O dielectric films on si(100) studied by quantitative analysis of reflection electron energy loss spectra, J. Appl. Phys. 100 (2006) 083713, http://dx.doi.org/10.1063/1.2360382.
[14] S. Tanuma, C.J. Powel, D.R. Penn, Calculation of electron inelastic mean free paths, Surf. Interface Anal. 20 (1993) 77–89, http://dx.doi.org/10.1002/sia.740200112.
[15] M. Vos, R. Moreh, K. Tőkési, The use of electron scattering for studying atomic momentum distributions: the case of graphite and diamond, J. Chem. Phys. 135 (2011) 024504, http://dx.doi.org/10.1063/1.3607993.
[16] M. Vos, C.A. Chatzidimitriou-Dreismann, T. Abdul-Redah, J. Mayers, Electron and neutron scattering from polymer films at high momentum transfer, Nucl. Instr. and Meth. B 227 (2005) 233–250, http://dx.doi.org/10.1016/j.nimb.2004.09.003.
[17] V.F. Sears, Scaling and final state interaction in deep inelastic neutron scattering, Phys. Rev. B 30 (1) (1984) 44, http://dx.doi.org/10.1103/PhysRevB.30.44.